Polarizable point-charge model for water: Results under normal and extreme conditions

Igor M. Svishchev, Peter G. Kusalik, Jian Wang,[a] and Russel J. Boyd
Department of Chemistry, Dalhousie University, Halifax, Nova Scotia B3H 4J3, Canada

(Received 16 April 1996; accepted 4 June 1996)

Molecular dynamics simulations of liquid water under normal and extreme conditions are performed using the polarizable point-charge (PPC) model. This efficient three-site model explicitly incorporates results from *ab initio* studies of the water molecule in applied electric fields. The structural, thermodynamic, and dielectric properties, and the self-diffusion coefficient are examined at a number of temperatures ranging from 263 to 573 K. These simulation results are compared with available experimental data along the liquid–vapor coexistence line; the agreement is very good for all properties studied. The temperature of maximum density for the PPC model is found to coincide with the experimentally observed value of 277 K. The spatial coordination of water molecules in the liquid and the anisotropy of the self-diffusion tensor are analyzed at various state points. Increased directional anisotropy in the local translational diffusion, suggestive of prenucleation phenomena, can be observed at $T=263$ K. Above $T=473$ K the local translational anisotropy becomes rather insensitive to temperature variation indicating a weakening of the correlations between water molecules. Rototranslational dynamics and nonlinear polarization effects arising in polarizable models for water are discussed along with their phenomenological implications. The dimer properties for the PPC potential are also reported. © *1996 American Institute of Physics.* [S0021-9606(96)51434-0]

I. INTRODUCTION

Simple point-charge models[1–7] are now used widely as condensed phase potentials in computer simulations of water. Two of the more popular and successful models are the extended single point-charge (SPC/E)[3] and TIP4P[2] potentials. These rigid nonpolarizable models incorporate three fixed charge sites in a single Lennard-Jones sphere; the effective pair potentials that result have been parametrized for ambient conditions. One of their major shortcomings is that the effects of electronic polarization which play an important role in physical–chemical processes in water are not explicitly included. Also, their ability to reproduce the behavior of real water over a wide range of state parameters is rather limited. In recent years considerable effort has been devoted to the development of more refined water models that explicitly incorporate polarizability,[7–16] including a nonempirical density functional based scheme.[17] However, a satisfactory polarizable model describing both the static and dynamic properties of water over a wide range of densities and temperatures is still lacking.

The traditional means of incorporating the nonadditive polarization effects into a classical water model has been to add point polarizabilities, the polarization centers being located at the atoms or on the OH bonds.[9,13] The interaction potential then includes additional terms involving the induced dipole moment,

$$\mathbf{p}=\alpha\cdot\mathbf{E}, \tag{1}$$

where α is the polarizability tensor and $\mathbf{E}$ is the local electric field. This local field includes contributions from all molecules in the system and is usually determined in a self-consistent manner using an iterative procedure. A variation on this method, due to Robinson and co-workers,[14] takes the polarization effect into account by allowing the values of the charges to vary according to the instantaneous local electric fields, where no iterations are used. A quite different approach (developed by Sprik and Klein[10]) treats polarizability as an explicit degree of freedom with an artificial inertial mass.

In the present molecular dynamics (MD) simulation study we examine the liquid state properties, both under normal and extreme conditions, of a new polarizable point-charge model for water. This polarizable model for water (hereafter the PPC model) retains most of the simplicity of the popular classical three-site models while incorporating the electrostatic response of the water molecule to a local electric field as determined from *ab initio* calculations. In our recent work on the virial equation of state for water the PPC potential was found to be far superior to standard effective potentials (such as TIP4P and SPC/E) in reproducing the second and the third virial coefficients for steam.[18] In the present study we demonstrate that both the static properties, such as the local structure, the internal energy, and the dielectric constant, and the dynamic properties, such as the self-diffusion coefficient and the Debye relaxation time, for liquid PPC water closely follow experimental data over a broad range of temperatures, from 263 to 573 K. The density

[a]Present address: Department of Pharmaceutical Chemistry, School of Pharmacy, University of California, San Francisco, CA 94143-0446.

 0021-9606/96/105(11)/4742/9/$10.00

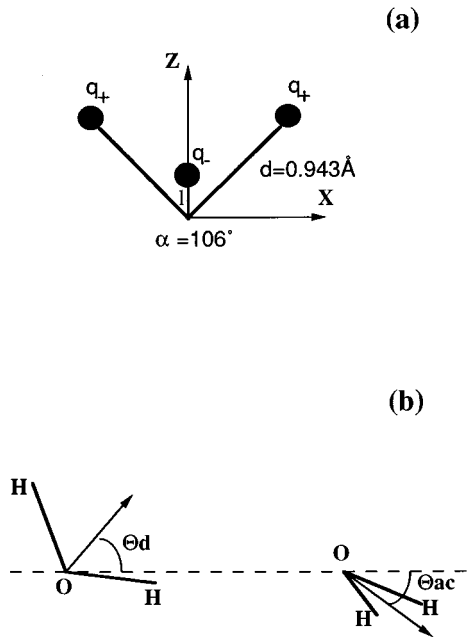

FIG. 1. (a) The geometry of the polarizable point-charge model and (b) the water dimer configuration.

maximum for liquid PPC water is observed at approximately 277 K, also in accord with experimental observations. Detailed analysis of the self-diffusion tensor and its temperature variations reveals an interesting connection between the spatial coordination of water molecules in the liquid and the directional anisotropy of their local translational motions.

The remainder of this paper is organized as follows. In Sec. II we describe our computer simulation methodology. In Sec. III we report the dimer properties, while in Sec. IV we present results for the liquid PPC water. Finally, our conclusions are summarized in Sec. V.

II. MODEL AND SIMULATION METHODOLOGY

Quantum-chemical calculations were carried out using GAUSSIAN 90[19] at the 6-31G** level[20] for a water molecule in the presence of homogeneous static electric field ranging in value from 0 to 3 V/Å. The molecular dipole moment and the values of atomic site charges, as obtained from natural population analysis, were recorded as functions of field strength and direction. For all but the largest fields an essentially linear response was observed. The polarization response of the molecule, now simply decomposed into three orthogonal (Cartesian) contributions, was parametrized in terms of the charges on its three sites and the position of the negative charge. The values of the hydrogen charges are given by

$$q_+ = 0.486 \pm 0.03E_X + 0.02E_Z, \tag{2}$$

where the sign of the X term changes with hydrogen 1 or 2, the electric field is given in V/Å, the Z direction is defined to be along the axis of symmetry, and the molecule lies in the XZ plane (see Fig. 1). The charge on the negative (oxygen) site follows from charge neutrality. The hydrogen sites are fixed at their positions in the optimized zero-field geometry shown in Fig. 1(a). The position (in Å) of the negative (oxygen) charge was parametrized to fit the observed field dependence of the dipole moment of the molecule and is given by

$$l_Z = 0.11 - 0.03E_Z \tag{3}$$

and

$$l_X = -0.025E_X. \tag{4}$$

In order to preserve the planar geometry of this simple three-site model, no Y polarization was considered; this assumption, also exploited by Berne and co-workers,[16] aids in the numerical implementation of this model. We point out that the PPC model incorporates an elevated value (2.14 D) for its zero-field molecular dipole moment and a smaller polarizability ($\alpha_X = 1.01$ Å^3 and $\alpha_Z = 0.66$ Å^3) when compared with real water, but these modifications appear to compensate one another for their effects.[21] The short-range interaction of the PPC model was taken to be a Lennard-Jones potential centered on the oxygen site. The Lennard-Jones parameters, $\epsilon = 0.6$ kJ/mol and $\sigma = 3.234$ Å, were optimized to give the correct energy, self-diffusion coefficient, and structure for water at 298 K.

Our molecular dynamics (MD) simulations were performed over a wide range of temperatures, from 263 to 573 K, both under constant density and constant pressure conditions, using experimental densities for water along the coexistence line and $P = 0$ atm, respectively. Except where explicitly stated, the results presented in Sec. IV are from constant density simulations. We have utilized a truncated octahedral simulation cell containing 256 particles in periodic boundary conditions.[22] The Ewald summation technique[23] was used to calculate the self-consistent electrostatic fields and the resulting electrostatic forces. Our implementation of the Ewald method can be found elsewhere.[24,25]

An algorithmic block-diagram for the algorithm employed in our MD simulations with the PPC model is given in Appendix A. Following the work of Ahlstrom *et al.*[9] a second-order predictor scheme was used to determine the instantaneous values of the electrostatic fields on molecules (at the oxygen site) prior to the iteration procedure. This scheme,

$$E(t_n) = 3.0E(t_{n-1}) - 3.0E(t_{n-2}) + E(t_{n-3}), \tag{5}$$

where t_n denotes the current time step, uses converged values from the previous time steps. The oxygen positions in the molecules were determined from Eqs. (3) and (4) (once at each time step) with these predicted values of the local electric fields. A standard iteration procedure was then applied (to the site charges) to calculate the self-consistent electrostatic fields. On average, three to four iterations were required every time step to calculate the self-consistent fields with the convergence criterion of

$$(\delta E)^2/\langle E^2 \rangle < 0.0003 \tag{6}$$

applied to each molecule. The efficiencies of some typical polarizable models for water are compared in Table I.

TABLE I. Computational efficiency of some polarizable water models.

Model	Number of force centers	Time step (fs)	Number of iterations per step
NCC[a]	3 charges+2 dipoles	0.5	6–9
PSPC[b]	3 charges+1 dipole	0.5	7–8
PPC	3 charges	1	3–4

[a]Reference 8.
[b]Reference 9.

Our isokinetic equations of motion were integrated using a fourth-order Gear algorithm[23] with the time step of 1.0 fs. Our systems were equilibrated for approximately 100 ps, and averages were collected over subsequent 300–500 ps trajectories. We remark that unlike other polarizable models, which typically execute at least 3–4 times more slowly than effective potential models, a comparable calculation with the PPC model runs only 1.5 times more slowly than a simulation with SPC/E water. This significant speed-up in our implementation of a polarizable model for water results partially from the fact that the site–site distances are determined only once at each time step, since the iteration procedure is applied only to the magnitudes of the charges and not to their positions. (We note that the absence of the Y polarizability in our three-site model precludes the out-of-plane displacements of the negative charges,[16] hence eliminating the necessity of the time-consuming reevaluation of the site–site separations after each iteration.) Another advantage of the PPC model is that it can utilize a ''regular'' time step.

III. DIMER PROPERTIES

The dimer properties for the PPC, SPC, and TIP4P potentials are compared in Table II. The binding energy, E_b, the oxygen–oxygen separation, R_{OO}, the donor and the acceptor angles, Θ_d and Θ_{ac}, respectively, are listed along with the experimental estimates. The geometric parameters for the dimer are defined in Fig. 1(b). In comparison with the effective pairwise additive models (such as SPC and TIP4P), which are known to give the dimer separation that is too small, the PPC model provides a more accurate description of the most stable dimer configuration. Previous workers[11,13,14] have similarly found polarizable models to be superior in reproducing the water dimer properties. We also remark that both the second and the third virial coefficients for the PPC model agree well with available experimental data, whereas these effective pair potentials fail to reproduce the virial equation of state for steam, particularly at lower temperatures.[18]

TABLE II. The dimer properties for various water models.

Model	E_b (kJ/mol)	R_{OO} (Å)	Θ_d	Θ_{ac}
SPC	−27.6	2.74	52°	22°
TIP4P	−26.1	2.75	52°	46°
PPC	−24.1	2.81	51°	25.5°
Expt.[a]	−22.7	2.976	51°	57°

[a]Reference 57.

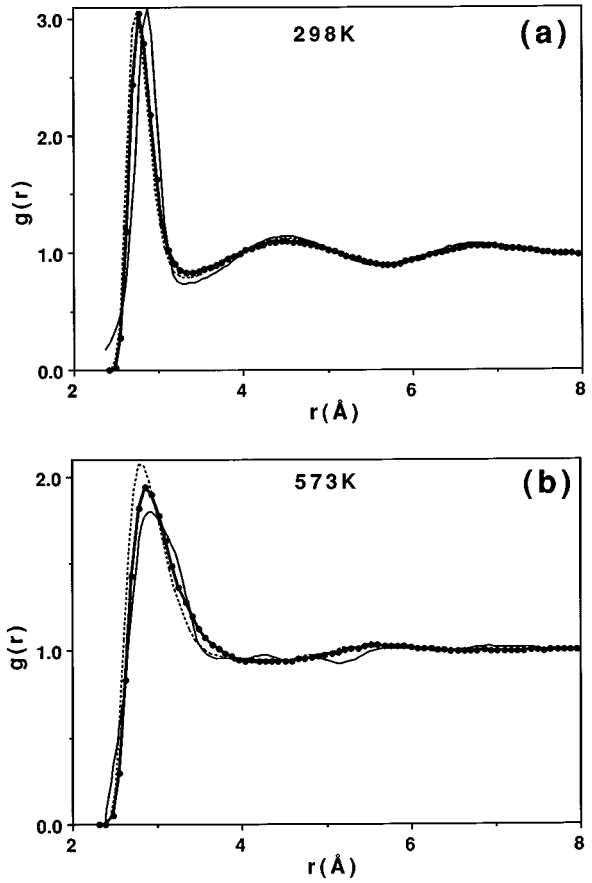

FIG. 2. The oxygen–oxygen radial distribution function for water at $T=298$ K (a) and 573 K (b). In (a) and (b) the PPC model is represented with the thick solid line with the dots, the dashed line represents SPC/E model results, and the thin solid line is the experimental curve.

IV. LIQUID WATER

A. Structure

The oxygen–oxygen radial distribution functions (RDF), $g_{OO}(r)$, for liquid PPC water at temperatures of 298 and 573 K are displayed, respectively, in Figs. 2(a) and 2(b). Also shown are experimental data,[26] as well as those obtained in simulations using the effective SPC/E potential. It can be seen from Fig. 2(a) that the PPC model is as successful as any standard nonpolarizable model at reproducing the orientationally averaged local structure in liquid water at ambient conditions. At higher temperatures the PPC model achieves better agreement with the experimental data, particularly in the region of the first-neighbor peak in the RDF [see Fig. 2(b)]. It is worth noting that many of the existing polarizable water potentials[11–14] have some difficulty in accurately reproducing the local structure in the liquid even under normal conditions, and no systematic tests of these potentials have been presented over a broad range of state parameters.

Figure 3 displays the out-of-plane component of the

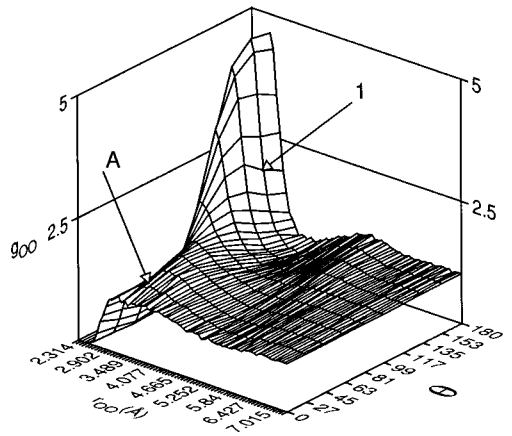

FIG. 3. The oxygen–oxygen spatial distribution function (φ=90°) for liquid PPC water at T=473 K. The first H-bond neighbors are denoted as 1 and the interstitial (nontetrahedral) coordination is marked with A. The local ordering essentially perpendicular to the plane of the water molecule is displayed.

oxygen–oxygen spatial distribution function (SDF), $g_{OO}(r,\Omega)$, for liquid PPC water at temperature of 473 K. The full SDF can be used to characterize the three-dimensional local coordination in this liquid.[27] We recall that $\Omega=(\theta,\varphi)$ denotes the angular coordinates of the separation vector, where θ is the angle between the dipole axis of the central water molecule and the oxygen–oxygen separation vector and φ is the angle away from the plane of this molecule.

As we might expect the nearest hydrogen (H) bond neighbor peaks in the SDF at 2.7–2.8 Å are considerably broadened at 473 K. We also find that, while the H-bond accepting molecules remain essentially in their tetrahedral positions in the local frame of the central molecule, the peaks due to H-bond donors change appreciably in their angular coordinates, these neighbors now preferentially appearing along the dipole axis of the central molecule (see Fig. 3). The second (H-bonded) neighbor peaks in the spatial pair-density distribution (around 4.5 Å) are nearly indiscernible. The interstitial peak in the SDF $g_{OO}(r,\Omega)$ due to nontetrahedral coordination,[27,28] which is clearly evident at lower temperatures at separations of 3.2–3.9 Å for some orientations, also undergoes a significant broadening and appears more as a shoulder on the first neighbor peak (see Fig. 3). This broadening of the interstitial distribution at high temperatures results in the rather featureless tail in the orientationally averaged RDF, $g_{OO}(r)$, beyond the first H-bond neighbor peak [see Fig. 2(b)]. At or below temperatures of 373 K both the secondary tetrahedral coordination and the interstitial coordination can be identified from the spatial pair-density distributions. Our analysis of the local spatial structure in liquid water under normal conditions can be found elsewhere.[27–29]

B. Thermodynamics

Following similar approaches for point-charge models for polar–polarizable molecules[3,6,10,30] we determined the average configurational energy as

$$\Delta U=\Delta U_q+\Delta U_{\rm pol}+\Delta U_{\rm LJ}. \tag{7}$$

TABLE III. The thermodynamic properties for the PPC model along the experimental coexistence line. The numerical uncertainty is estimated at 0.2%.

T (K)	ρ (g/cm^3)	ΔU (kJ/mol)[a]	$\Delta U_{\rm exp}$ (kJ/mol)
263	0.9981	−44.0	−44.7
298	0.9970	−41.4	−41.5
373	0.9583	−37.3	−37.3
473	0.8647	−31.5	−31.4
573	0.7123	−24.2	−22.2

[a]Includes a permanent self-energy correction of 1.8 kJ/mol.

In this expression

$$\Delta U_q=\frac{1}{2}\sum_k^{{\rm on}i}\sum_l^{{\rm on}j}\frac{q_k q_l}{r_{kl}} \tag{8}$$

is the total electrostatic term in which the summation runs over the (perturbed) site charges (k,l) of the molecules (i,j), and

$$\Delta U_{\rm pol}=\frac{1}{2}\sum_\beta\sum_i\frac{(\mu_{i,\beta}-\mu_{0,\beta})^2}{\alpha_\beta} \tag{9}$$

is the polarization term which accounts for the work done in distorting the molecule [$\mu_{i,\beta}$ and $\mu_{0,\beta}$ are the principal components of the dipole moment of the PPC molecules in condensed phase and in zero-field conditions, respectively, α_β are the principal components of the polarizability tensor for the PPC model, and $\beta=(x,z)$]. In Eq. (9)

$$\Delta U_{\rm LJ}=\frac{1}{2}\sum_{ij}4\epsilon_{\rm LJ}\left[\left(\frac{\sigma}{\mathbf{r}_{ij}}\right)^{12}-\left(\frac{\sigma}{\mathbf{r}_{ij}}\right)^{6}\right] \tag{10}$$

is the Lennard-Jones term acting between the oxygen sites. To account for the difference between the elevated zero-field dipole moment (2.14 D) for the PPC model and the actual gas phase dipole moment (1.85 D) of the water molecule in comparing our estimates for the liquid state configurational energy with the experimental values a permanent self-term polarization correction (analogous to that employed in Ref. 3) of 1.8 kJ/mol was added to our simulation results from Eq. (7).

The experimental energy for liquid water was obtained from the relationship[2]

$$\Delta H_{\rm vap}=-\Delta U+P\Delta V, \tag{11}$$

where $\Delta H_{\rm vap}$ is the heat of vaporization, P is the pressure, and ΔV is the volume difference between liquid and vapor phases. The necessary experimental data along the coexistence curve were taken from Ref. 31.

The calculated and the experimental values for the average configurational energy are compared in Table III. The agreement is very good; the values are typically within 1%, with the exception of the T=573 K state point where the discrepancy is approximately 8%.

TABLE IV. The dielectric properties for the PPC model along the experimental coexistence line. The numerical uncertainty in τ_D is estimated at 10%. The numerical uncertainty in ϵ is shown explicitly in Fig. 5.

T (K)	ϵ	μ (D)	τ_D (ps)
263	109	2.53	31.6
298	77	2.51	8.9
373	55	2.45	2.3
473	41	2.39	0.91
573	22	2.34	0.62

C. Static and time-dependent dielectric properties

The dielectric constants in this study were calculated using the appropriate fluctuation formula for a polar–polarizable fluid in Ewald boundary conditions[32,33]

$$\frac{(\epsilon-\epsilon_\infty)(2\epsilon_{\rm rf}+1)^2}{(2\epsilon_{\rm rf}+\epsilon)(2\epsilon_{\rm rf}+\epsilon_\infty)}=\frac{4\pi}{3}\frac{\langle M^2\rangle}{VkT}. \tag{12}$$

In this expression M and V are, respectively, the total dipole moment and the volume of the simulation cell, $\epsilon_{\rm rf}$ is the dielectric constant of the surrounding continuum, and ϵ_∞ is the high-frequency dielectric constant. In our calculations the value of $\epsilon_{\rm rf}$ was taken to be that of real water at the temperature of interest and $\epsilon_\infty=1.25$ was obtained from the Clausius–Mossotti formula[34,35]

$$\frac{(\epsilon_\infty-1)}{(\epsilon_\infty+2)}=\frac{4\pi}{3}\frac{N}{V}\alpha, \tag{13}$$

where α represents the mean polarizability for the PPC model.

The static dielectric constants for liquid PPC water obtained from our simulation runs are given in Table IV and are compared with experimental data[36] in Fig. 4. The agreement is very good over the entire temperature range studied. Also shown in Fig. 4 are the dielectric constants for the SPC/E model.[37,38] The inset in Fig. 4 displays the temperature dependence for the average liquid-state molecular dipole moment obtained in this work. The liquid-state dipole moments are substantially elevated above the zero-field value with the result at room temperature concurring with previous estimates.[39]

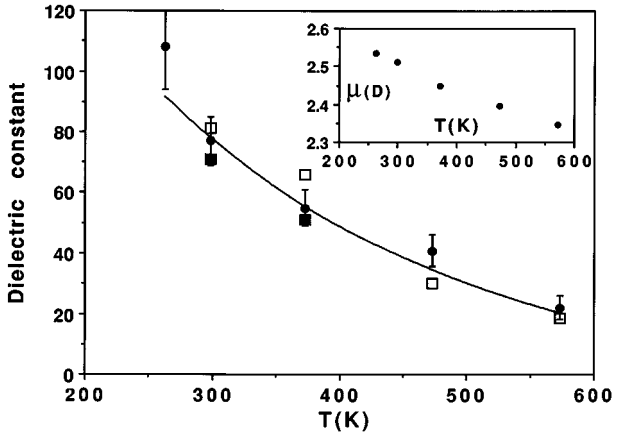

FIG. 4. The static dielectric constant for liquid water. The simulation results for the PPC model (the circles) and SPC/E water (open and full squares represent data from Refs. 37 and 38, respectively) are compared with experimental data (solid line) along the coexistence curve. The inset shows the temperature dependence of the average dipole moment of PPC molecules.

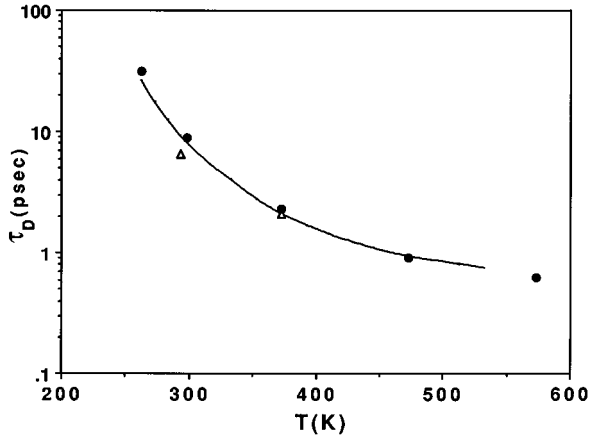

FIG. 5. The Debye relaxation time for liquid water. Simulation results for the PPC and TIP4P models (the circles and the triangles, respectively) are compared with experimental data (solid line) along the coexistence curve.

We have also determined the collective relaxation times, τ, for PPC water,

$$\tau=\int_0^\infty \frac{\langle \mathbf{M}(t)\mathbf{M}(0)\rangle}{M^2}\,dt, \tag{14}$$

from the integration of the corresponding total dipole moment autocorrelation functions (ACFs). In this study direct numerical integration of the total dipole moment ACFs was performed at short and intermediate times; the long-time tails were approximated with the appropriate exponential function and were integrated analytically. Using these simulation data we have estimated the Debye relaxation times, τ_D, which can be determined from the low-frequency limit of the frequency-dependent dielectric constant[25,35]

$$\tau_D=\lim_{\omega\to\infty}\frac{1}{i\omega}\frac{\epsilon-\epsilon(\omega)}{\epsilon(\omega)-\epsilon_\infty}=\frac{2\epsilon_{\rm rf}+\epsilon}{2\epsilon_{\rm rf}+\epsilon_\infty}\,\tau. \tag{15}$$

Our estimates for the Debye relaxation times are included in Table IV and are compared with the available experimental data[40] and results from the TIP4P model[41] in Fig. 5. We find that the PPC model accurately describes the process of dielectric relaxation in water along the entire liquid–vapor coexistence line.

D. Self-diffusion coefficient and its anisotropy

In this study we have also determined the mean translational self-diffusion coefficient and its principal components for liquid PPC water, and have analyzed their temperature variations. The principal components, D_β, of the self-diffusion coefficient have been calculated by integrating the appropriate velocity autocorrelation functions in the local molecular frame.[24,42] This is expressed as

TABLE V. The self-diffusion coefficients for the PPC model along the experimental coexistence line. The numerical uncertainty is estimated at 2%.

T (K)	D (10^{-5} cm/s^2)	D_x (10^{-5} cm/s^2)	D_y (10^{-5} cm/s^2)	D_z (10^{-5} cm/s^2)
263	0.95	0.8	1.41	0.60
298	2.6	2.4	3.56	1.81
373	9.6	9.25	12.6	7.80
473	18.8	18.1	21.3	16.4
573	33.2	32.4	38.3	29.1

$$D_\beta = \int_0^\infty \langle [\mathbf{v}_\beta(0)\cdot\mathbf{e}_\beta(0)][\mathbf{v}_\beta(t)\cdot\mathbf{e}_\beta(0)]\rangle dt, \tag{16}$$

where $\mathbf{e}_\alpha$ are the unit vectors of the principal frame ($\beta=x$, y and z) and $\mathbf{v}_\beta(t)\cdot\mathbf{e}_\beta(0)$ is the β-component of the center-of-mass velocity defined in the local frame at $t=0$. The mean translational self-diffusion coefficient, D, can then be expressed as

$$D = 1/3(D_x + D_y + D_z). \tag{17}$$

Calculated values for these quantities are given in Table V and are compared with the available experimental estimates[43] and the results for the TIP4P[42] and SPC/E[37] models in Fig. 6(a). The agreement between the simulation results for the PPC model and the experimental data is typically within 10%–15% for all the state points examined.

Figure 6(b) examines the directional anisotropy in the local translational diffusion, as characterized by the ratios of D_β/D, for the PPC and TIP4P models at different temperatures. We find that nonpolarizable water models such as TIP4P exhibit a smaller anisotropy in the self-diffusion coefficient than our polarizable model. It can be seen in Fig. 6(b) that in the low-temperature region, near $T=263$ K, the anisotropy in D tends to increase rapidly in both liquids. This increase in the directional anisotropy of the translational diffusion was found to accompany the crystallization phenomena in supercooled liquid carbon dioxide,[44] however we did not observe nucleation in liquid PPC water at 263 K over a period of 1 ns. We remark that the field-induced crystallization of TIP4P water has been recently observed for a narrow range of temperatures and densities.[45,46] An important question to be addressed in future studies is whether spontaneous crystallization can be achieved under field-free conditions on a time scale of a typical simulation using a polarizable water model.

Another interesting trend which can be seen in Fig. 6(b) is that the ratios of D_β/D for liquid PPC water do not change significantly at temperatures beyond 473 K. We recall (see Sec. IV A) that dramatic structural changes have occurred in the spatial coordination of water molecules when a temperature of 473 K is reached where both the secondary tetrahedral features and the interstitial peaks have essentially disappeared from the spatial distribution $g_{OO}(r,\Omega)$. At the same time, some directional anisotropy in the translational motions still persists at these high temperatures (i.e., these ratios are not equal to one), presumably due to the influence of the nearest H-bond neighbors.

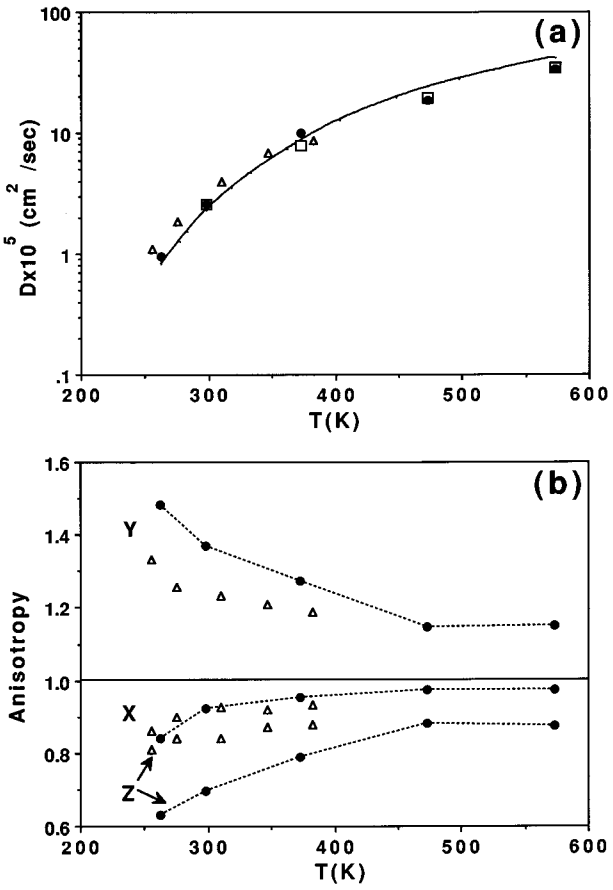

FIG. 6. The self-diffusion coefficient for liquid water. In (a) the mean self-diffusion coefficients for the PPC, TIP4P, and SPC/E models (the full circles, the open triangles, and the open squares, respectively) are compared with experimental data (solid line) along the coexistence curve. In (b) the relative anisotropies in the self-diffusion coefficient for the PPC and TIP4P models (indicated by full circles and open triangles, respectively) are displayed. The data represent the ratios of $D_{(x,\ y,\ \text{or}\ z)}/D$.

E. Density maximum

The density maximum is among the most characteristic of the thermodynamic anomalies[47] associated with liquid water and its location represents a crucial test for any potential model. We have determined the density maximum for liquid PPC water using constant pressure MD simulations. Our results at zero pressure are plotted against the experimental densities for water in Fig. 7. A simple polynomial fit to the simulation data between 268 and 298 K puts the density maximum for the PPC model at 277 K, which is also the experimentally observed temperature. Clearly, the PPC potential is capable of a relatively accurate description of many of the major static and dynamic properties of liquid water from its supercooled to near-critical states.

F. Induced polarization and rototranslational coupling

An interesting feature in the optical spectra for liquid water is the presence of a low-lying rototranslational mode at $\sim$200 cm^{-1}.[48–51] This mode is rather weak in the power spectra of various auto- and cross-correlation functions for nonpolarizable water models which has led to the previous

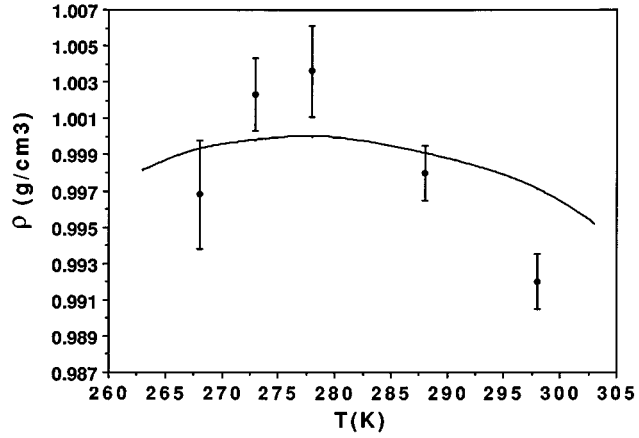

FIG. 7. The dependence of the density on temperature at $P=0$. Simulation results for the PPC model (the circles) are compared with experimental data (solid line).

assertion that its prominence in experimental optical spectra is due to interaction-induced polarization effects.[52–55] In this study we have calculated the power spectra of the nonvanishing cross-correlation functions between the linear and angular velocities, $\langle v_x(t)\omega_y(0)\rangle$ and $\langle v_y(t)\omega_x(0)\rangle$, for our explicitly polarizable PPC model. The results are shown in Fig. 8, where they are compared with those obtained for the nonpolarizable SPC/E model.[29] Examination of the PPC spectra reveals peaks at about 500 and 750 cm^{-1} (due to coupling with librational motions) and a peak at $\sim$60 cm^{-1} arising from low frequency translational modes. The spectra for the PPC model exhibit a much more intense mode at about 200 cm^{-1} than is observed for SPC/E water, which supports the claim that its presence in the experimental spectra is largely due to the induced polarization effects accompanying rototranslational dynamics in liquid water.

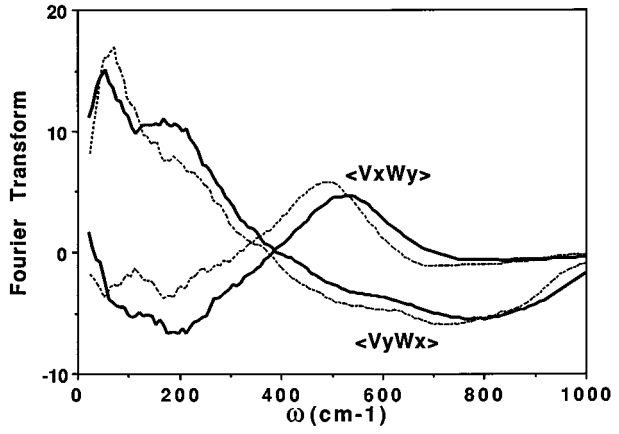

FIG. 8. The power spectra of the cross-correlation functions $\langle v_x(t)\omega_y(0)\rangle$ and $\langle v_y(t)\omega_x(0)\rangle$ for PPC (solid line) and SPC/E (dashed line) water at 298 K.

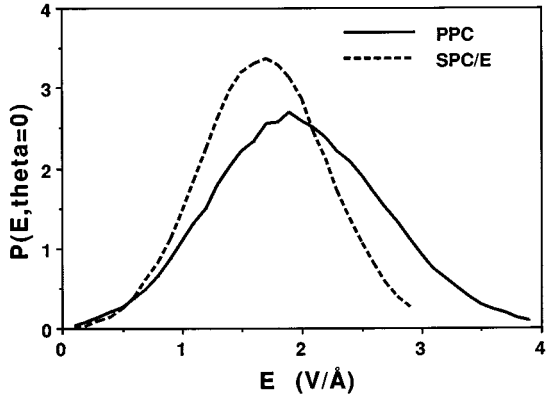

FIG. 9. The probability distribution for the magnitude of the local electric field along the molecular dipole axis for PPC and SPC/E water at 298 K.

G. Nonlinear polarization effects

In order to investigate the importance of nonlinear polarization effects, we have generated the probability distribution function, $P(E,\theta)$, in which E is the magnitude of the local electric field and θ is the angle between the field vector and the molecular dipole axis. This distribution is a maximum at $\theta=0$, and hence at Fig. 9 we have presented $P(E,\theta=0)$ for PPC and SPC/E water at 298 K. It is clear from Fig. 9 that the fluctuations in the magnitude of the local electric field are suppressed in the effective SPC/E model. In PPC water we observe that there is a nontrivial probability of the local field being in excess of 3 V/Å. At such large fields, nonlinear effects can be expected to become more significant, accounting for about 10% of the polarization response.[56] We might expect these rare but large local field fluctuations to be of importance in the phase behavior of liquid water,[46,47] a conjecture yet to be fully explored in simulation studies. We remark that the average local electric fields have magnitudes of at least 1.5 V/Å in SPC/E and PPC water at 298 K. This field strength is equivalent to that which is experienced at about 3 Å from a unit charge.

V. CONCLUDING REMARKS

Explicit inclusion of electronic polarization is essential for a classical water model which aims to provide an accurate description over a wide range of state points. In this work we have demonstrated that the polarizable point-charge (PPC) model reproduces both the static and the dynamic properties of liquid water from supercooled to near-critical conditions. In another recently published study this simple three-site model has been successfully exploited in reproducing the virial equation of state for steam.

The average local structure, the internal energy, the static dielectric constant, the Debye relaxation time, and the self-diffusion coefficient for the PPC model have been examined in molecular dynamics simulations. These simulations have been carried out along the experimental liquid–vapor coexistence line at temperatures from 263 to 573 K. Excellent agreement with the available experimental data has

been achieved. We have also determined the density maximum for this model; at ambient pressure it appears at $T \approx 277$ K, in accord with experimental observations.

The principal components of the self-diffusion coefficient for the PPC model have been determined using the appropriate center-of-mass velocity autocorrelation functions resolved in the local molecular frame. We have demonstrated that the directional anisotropy in the local translational motions can be directly related to the specific spatial coordinations of water molecules arising in the liquid at various temperatures.

In this study the power spectra of the nonvanishing cross-correlation functions between the linear and angular velocities for the PPC model have been obtained. Comparison with the effective SPC/E model reveals that our polarizable model exhibits a much more intense rototranslational mode at about 200 cm^{-1}. It implies that the induced polarization effects which accompany the rototranslational motions of water molecules are largely responsible for its presence in the experimental optical spectra.

Finally, we have examined the distribution of the local electric fields experienced by water molecules in the liquid state. The presence of rather large local fields (in excess of 3 V/Å) is observed in PPC water, while in the effective SPC/E model the fluctuations in the magnitude of the local electric field are suppressed.

ACKNOWLEDGMENTS

We are grateful for the financial support of the Natural Sciences and Engineering Research Council of Canada. J. W. thanks Killam Trust for a Predoctoral Fellowship.

APPENDIX A: SIMULATION ALGORITHM

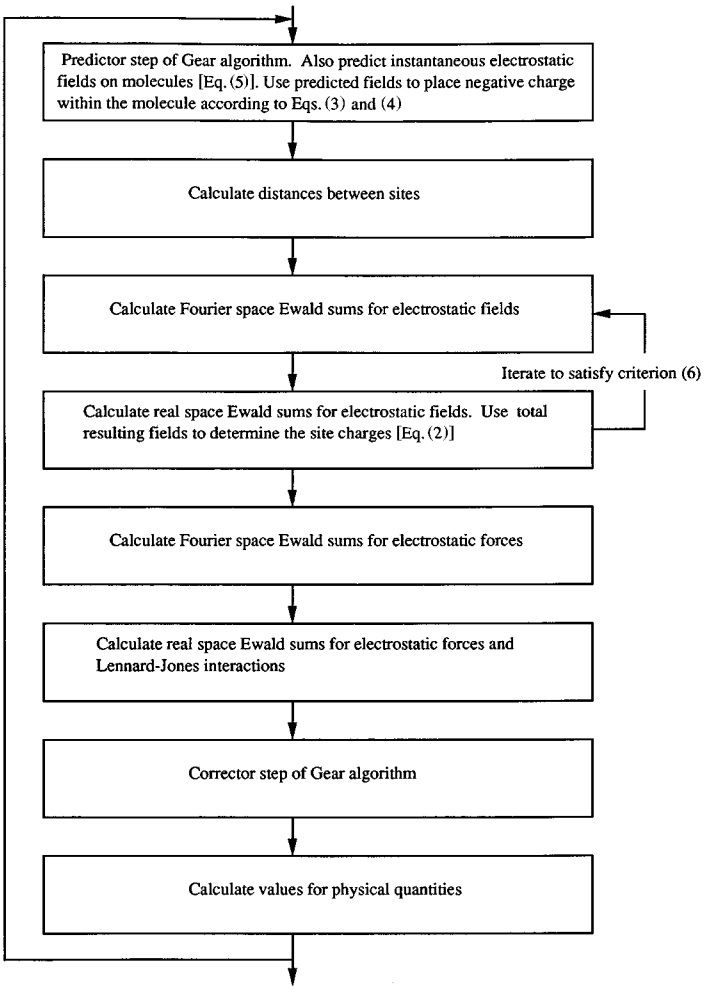

[1] F. H. Stillinger and A. Rahman, J. Chem. Phys. **60**, 1545 (1974).
[2] W. L. Jorgensen, J. Chandrasekhar, J. D. Madura, R. W. Impey, and M. L. Klein, J. Chem. Phys. **79**, 926 (1983).
[3] H. J. C. Berendsen, J. R. Grigera, and T. P. Straatsma, J. Phys. Chem. **91**, 6269 (1987).
[4] H. L. Lemberg and F. H. Stillinger, J. Chem. Phys. **62**, 1677 (1975).
[5] J. R. Reimers, R. O. Watts, and M. L. Klein, Chem. Phys. **64**, 95 (1982).
[6] K. Watanabe and M. L. Klein, Chem. Phys. **131**, 157 (1989).
[7] S.-B. Zhu, S. Singh, and G. W. Robinson, Adv. Chem. Phys. **85**, 627 (1994).
[8] U. Niesar, G. Corongiu, E. Clementi, G. R. Kneller, and D. K. Bhattacharya, J. Phys. Chem. **94**, 7949 (1990).
[9] P. Ahlström, A. Walquist, S. Engström, and B. Jönsson, J. Mol. Phys. **68**, 563 (1989).
[10] M. Sprik and M. L. Klein, J. Chem. Phys. **89**, 7556 (1988).
[11] P. Cieplak, P. Kollman, and T. Lybrand, J. Chem. Phys. **92**, 6755 (1990).
[12] R. E. Kozack and P. C. Jordan, J. Chem. Phys. **96**, 3120 (1992).

[13] D. N. Bernardo, Y. Ding, K. Krogh-Jespersen, and R. M. Levy, J. Phys. Chem. **98**, 4180 (1994).
[14] S.-B. Zhu, S. Singh, and G. W. Robinson, J. Chem. Phys. **95**, 2791 (1991).
[15] J. W. Halley, J. R. Rustad, and A. Rahman, J. Chem. Phys. **98**, 4110 (1993).
[16] S. W. Rick, S. J. Stuart, and B. J. Berne, J. Chem. Phys. **101**, 614 (1994).
[17] K. Laasonen, M. Sprik, M. Parrinello, and R. Car, J. Chem. Phys. **99**, 9080 (1993).
[18] P. G. Kusalik, F. Liden, and I. M. Svishchev, J. Chem. Phys. **103**, 10169 (1995).
[19] M. J. Frisch, M. Head-Gordon, G. W. Trucks, G. B. Foresman, H. B. Schlegel, K. Raghavachari, M. A. Robb, J. S. Binkley, C. Gonzalez, D. J. Defrees, D. J. Fox, R. A. Whiteside, R. Seeger, C. F. Melius, J. Baker, R. L. Martin, L. R. Kahn, J. J. P. Stewart, S. Topiol, and J. A. Pople, GAUSSIAN 90, Gaussian, Inc., Pittsburgh, PA, 1990.
[20] Our choice of this modest basis set was dictated by a necessity to perform a large number of individual *ab initio* calculations (in excess of 50) with varying geometry and magnitude of the applied electric field.
[21] A reparametrization of the model was attempted in which the reproduction of the experimental gas-phase dipole moment and polarizability of the water molecule was enforced. This ''fully'' polarizable three-site model was less successful in reproducing the targeted condensed phase properties, while also requiring switching functions and nonlinear terms to handle the very large induced dipole moments arising in some liquid configurations.
[22] D. Fincham and D. M. Heyes, Adv. Chem. Phys. **63**, 493 (1985).
[23] M. P. Allen and D. J. Tildesley, *Computer Simulations of Liquids* (Oxford University Press, Oxford, 1987).
[24] I. M. Svishchev and P. G. Kusalik, J. Phys. Chem. **98**, 728 (1994).
[25] P. G. Kusalik, J. Chem. Phys. **93**, 3520 (1990).
[26] A. K. Soper and M. G. Phillips, Chem. Phys. **107**, 47 (1986).
[27] I. M. Svishchev and P. G. Kusalik, J. Chem. Phys. **99**, 3049 (1993).
[28] P. G. Kusalik and I. M. Svishchev, Science **265**, 1219 (1994).
[29] I. M. Svishchev and P. G. Kusalik, Chem. Phys. Lett. **215**, 596 (1993).
[30] F. H. Stillinger, J. Chem. Phys. **71**, 1647 (1979).
[31] *Proceedings of the 12th International Conference on the Properties of Water and Steam* (Begell House, New York, 1995), p. A 143.
[32] C. J. F. Böttcher, *Theory of Electric Polarization*, 2nd ed. (Elsevier, New York, 1973).
[33] M. Neumann, Mol. Phys. **50**, 841 (1983).
[34] H. Fröhlich, *Theory of Dielectrics* (Oxford University Press, Oxford, 1958).
[35] W. T. Coffey and Yu. P. Kalmykov, Chem. Phys. **169**, 165 (1993).
[36] In Ref. 31, p. A 132.
[37] Y. Guissiani and B. Guillot, J. Chem. Phys. **98**, 8221 (1993).
[38] M. R. Reddy and M. Berkowitz, Chem. Phys. Lett. **155**, 173 (1989).
[39] M. Sprik, J. Chem. Phys. **95**, 6763 (1991).
[40] O. A. Nabokov and Y. A. Lubimov, Mol. Phys. **65**, 1473 (1988).
[41] M. Neumann, J. Chem. Phys. **85**, 1567 (1986).
[42] R. Frattini, M. Sampoli, M. A. Ricci, and G. Ruocco, J. Chem. Phys. **92**, 2540 (1990).
[43] Z. H. Weingartner, Phys. Chem. Neue Folge **123**, 129 (1982).
[44] I. M. Svishchev and P. G. Kusalik, Phys. Rev. Lett. **75**, 3289 (1995).
[45] I. M. Svishchev and P. G. Kusalik, Phys. Rev. Lett. **73**, 975 (1994).
[46] I. M. Svishchev and P. G. Kusalik, J. Am. Chem. Soc. **118**, 649 (1996).
[47] R. J. Speedy and C. A. Angell, J. Chem. Phys. **65**, 851 (1976).
[48] G. E. Walrafen, J. Chem. Phys. **40**, 3249 (1964).
[49] H. R. Zelsmann, J. Mol. Struct. **350**, 95 (1995).
[50] K. Mizoguchi, Y. Hori, and Y. Tominaga, J. Chem. Phys. **97**, 1961 (1992).
[51] S. Krishnamurthy, R. Bansil, and J. Wiafe-Akenten, J. Chem. Phys. **79**, 5862 (1983).
[52] P. A. Madden and R. W. Impey, Chem. Phys. Lett. **123**, 502 (1986).
[53] R. Frattini, M. Sampoli, M. A. Ricci, and G. Ruocco, Chem. Phys. Lett. **141**, 297 (1987).
[54] F. Sciortino and G. Corongiu, Mol. Phys. **79**, 547 (1993).
[55] B. Guillot, J. Chem. Phys. **95**, 1543 (1991).
[56] G. Maroulis, J. Chem. Phys. **94**, 1182 (1991).
[57] J. A. Odutola and T. R. Dyke, J. Chem. Phys. **72**, 5062 (1980).